CHEMISTRY OF MATERIALS

Article

pubs.acs.org/cm

Postsynthetic Exchanges of the Pillaring Ligand in Three-Dimensional Metal–Organic Frameworks

Seok Jeong,[†] Dongwook Kim,[†] Xiaokai Song,[†,‡] Min Choi,[†] Noejung Park,*[,†] and Myoung Soo Lah*[,†]

[†]Interdisciplinary School of Green Energy, Ulsan National Institute of Science & Technology, Ulsan 689-805, Korea

[‡]Department of Chemistry and Applied Chemistry, Hanyang University, Ansan, Kyunggi-do 426-791, Korea

Supporting Information

ABSTRACT: Metal–organic frameworks, [Ni(HBTC)(dabco)] (**2**) and $[Ni_2(HBTC)_2(bipy)_{0.6}(dabco)_{1.4}]$ (**3**) (where H_3BTC is 1,3,5-benzenetricarboxylic acid, dabco is 1,4-diazabicyclo[2.2.2]octane, and bipy is 4,4′-bipyridine), were prepared via postsynthetic ligand exchanges of [Ni(HBTC)(bipy)] (**1**). By controlling the concentration of dabco, we could obtain not only entropically favorable **2** with completely exchanged dabco but also enthalpically favorable **3** with selectively exchanged bipy/dabco in the alternating layers.

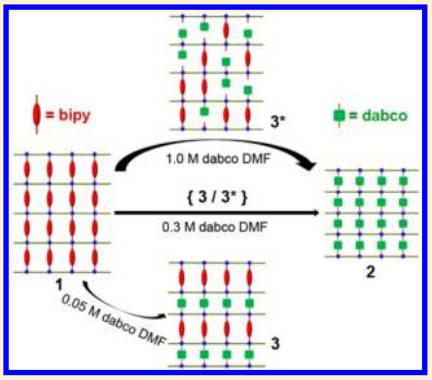

KEYWORDS: *metal–organic frameworks (MOFs), postsynthetic modification (PSM), postsynthetic ligand exchange (PSLE), enthalpically favorable exchange, entropically favorable exchange, gas sorption, adsorption enthalpy*

INTRODUCTION

Postsynthetic modification (PSM) of a metal–organic framework (MOF) is a convenient synthetic approach for the preparation of new isoreticular MOFs that are difficult to obtain or cannot be attained via the conventional synthetic approaches.[1] Systematic modifications of the reactive residue of an organic linker in a MOF could lead to new isoreticular MOFs with systematically varied characteristics. Recently, a new type of dative PSM, postsynthetic exchange of a structural component that was directly participating in the network connectivity, was reported.[2,3] The postsynthetic ligand exchange (PSLE) led to a new isoreticular MOF with a reduced pore dimension accompanied via one-dimensional reorganization of the framework structure[3a] and a hybrid MOF with mixed linker ligands of the same length in a single framework without any reorganization of the framework structure.[3b]

Recently, there was a report about the solvothermal preparation of a three-dimensional (3D) MOF, [Ni(HBTC)(bipy)] (**1**) (where H_3BTC is 1,3,5-benzenetricarboxylic acid and bipy is 4,4′-bipyridine).[4] In the network structure, both Ni^{II} ion and HBTC ligand as 3-connected nodes formed two-dimensional (2D) sheets of a honeycomb (**hcb**) net topology, and the 2D sheets are further pillared using 2-connected bipy linkers via the metal nodes to form a 3D network structure.

Here, we report the PSLE of **1** toward new isoreticular MOFs, [Ni(HBTC)(dabco)] (**2**) and $[Ni_2(HBTC)_2(bipy)_{0.6}(dabco)_{1.4}]$ (**3**) (where dabco is 1,4-diazabicyclo[2.2.2]octane), that cannot be attained via the conventional one-step synthetic approach. By controlling the concentration of dabco in *N*,*N*′-dimethylformamide (DMF), we could obtain not only **2** with completely exchanged pillaring layers via random exchange of a bipy linker but also **3** with alternatively exchanged pillaring layers via selective exchange. The relationship between the pore dimension and the sorption properties of the MOFs, such as adsorbate uptake amount and adsorption enthalpy, has been investigated.

EXPERIMENTAL SECTION

General Procedures. All reagents were purchased from commercial sources and used without further purification. Elemental analysis (EA) (C, H, and N) was performed at the Central Research Facilities of the Ulsan National Institute of Science & Technology. Powder X-ray diffraction (PXRD) data were recorded using a Bruker D2 Phaser automated diffractometer at room temperature, with a step size of $2\theta = 0.02°$. Simulated PXRD patterns were calculated using the Material Studio software package[5] employing a structural model from single-crystal data.

Preparation of MOF [Ni(HBTC)(bipy)], 1. **1** was prepared via a solvothermal reaction that was slightly modified from the reported synthetic procedures.[4] A mixture of $Ni(NO_3)_2{\cdot}6H_2O$ (37.8 mg, 0.130 mmol), H_3BTC (23.2 mg, 0.110 mmol), and bipy (17.2 mg, 0.110 mmol) was dissolved in a mixed solvent of 4 mL of DMF and 4 mL of MeOH, and the solution was divided into two portions. Each portion was transferred to a 10 mL vial. The tightly sealed vial was heated at 70 °C for 2 days to form cyan hexagonal crystals. The crystals of **1** were

Received: November 9, 2012
Revised: March 12, 2013
Published: March 13, 2013

   dx.doi.org/10.1021/cm303624p | *Chem. Mater.* 2013, 25, 1047–1054

harvested and washed using DMF and then air-dried at ambient temperature for a couple of hours. The activated sample, **1a**, was prepared by vacuum drying overnight at 150 °C. EA was performed on the sample of **1a**, which had been reexposed to air for a couple of hours. EA calcd for $[Ni(HBTC)(bipy)]\cdot 2H_2O$ ($C_{19}H_{16}N_2O_8Ni$, fw = 459.03 g/mol). Calcd: C, 49.71%; H, 3.51%; N, 6.10%. Found: C, 49.84%; H, 4.00%; N, 6.62%.

PSLE of 1. Before ligand exchange of the MOF, the as-synthesized single crystals of **1** were soaked in DMF for a couple of days to remove any remaining reactants and side products present in the solvent cavities. After the solvent had been decanted, the crystals were air-dried at ambient temperature for a couple of hours.

[Ni(HBTC)(dabco)], 2. Approximately 10 mg of the crystals of **1** presoaked in DMF was transferred to a vial of 10 mL of a 1.0 M dabco DMF solution, and the solution in the tightly sealed vial was stored for 2 days in an oven at 100 °C. The crystals slowly changed color from cyan to pale yellow while retaining their crystallinity during the soaking. The harvested crystals were air-dried at ambient temperature for a couple of hours. The activated sample, **2a**, was prepared by vacuum drying **2** at 150 °C overnight. EA was performed on the sample of **2a** reexposed in air for a couple of hours. EA calcd for $[Ni(HBTC)(dabco)]\cdot 2H_2O$ ($C_{15}H_{20}N_2O_8Ni$, fw = 415.02 g/mol). Calcd: C, 43.41%; H, 4.86%; N, 6.75%. Found: C, 42.98%; H, 4.97%; N, 6.95%.

$[Ni_2(HBTC)_2(bipy)_{0.6}(dabco)_{1.4}]$, 3. The PSLE procedure for the preparation of **3** was the same as that for **2** except for the use of a 0.05 M dabco DMF solution for 3 days. The pale green crystals were harvested and washed using DMF and then air-dried at ambient temperature for a couple of hours. The activated sample, **3a**, was prepared by vacuum drying **3** at 150 °C overnight. EA was performed on the sample of **3a** that had been reexposed to air for a couple of hours. EA calcd for $[Ni_2(HBTC)_2(bipy)_{0.6}(dabco)_{1.4}]\cdot 5H_2O$ ($C_{32.4}H_{39.6}N_4O_{17}Ni_2$, fw = 874.47 g/mol). Calcd: C, 44.50%; H, 4.56%; N, 6.41%. Found: C, 44.21%; H, 4.77%; N, 6.82%.

$[Ni_2(HBTC)_2(bipy)(dabco)]$, 4. The crystals of **4** were prepared by soaking approximately 30 mg of **3** in 10 mL of a 0.1 M bipy DMF solution at ambient temperature for 7 days. EA was conducted on the activated sample that had been reexposed to air for a couple of hours, where the activated sample was prepared by soaking the crystals in fresh DMF for 2−3 days and methylene chloride for 1 day and then vacuum drying at ambient temperature overnight. EA calcd for $[Ni_2(HBTC)_2(bipy)(dabco)]\cdot 7.5H_2O$ ($C_{34}H_{43}N_4O_{19.5}Ni_2$, fw = 937.11 g/mol). Calcd: C, 43.58%; H, 4.63%; N, 5.98%. Found: C, 43.17%; H, 5.08%; N, 6.30%.

Crystallographic Data Collection and Refinement of the Structure. Crystals of **2**−**4** were coated with Paratone oil, and the diffraction data were measured at 173 K using Mo Kα radiation in an X-ray diffraction camera system using an imaging plate equipped with a graphite crystal incident beam monochromator. The Rapid Auto software package[6] was used for data collection and processing. All structures were determined using direct methods employing SIR2008.[7] The structures were refined using full-matrix least-squares calculations employing the XL program of the SHELXTL PLUS software package.[8]

$[Ni_2(HBTC)_2(dabco)_2]$, 2. One-quarter of a nickel ion on a crystallographic *m*2*m* site, one-twelfth of a BTC^{3-} ligand on a crystallographic −62*m* site, one-sixth of a $H_{1.5}BTC^{1.5-}$ ligand on a crystallographic −6 site, and one-quarter of a pillaring dabco ligand on a crystallographic *m*2*m* site were observed as an asymmetric unit of hexagonal space group *P*-62*m*. All non-hydrogen atoms were refined anisotropically; the hydrogen atoms were assigned isotropic displacement coefficients $U(H) = 1.2U(C)$, and their coordinates were allowed to ride on their respective atoms. The final refinement was performed with modification of the structural factors for the electron densities of the disordered solvent region (744 Å^3, 44.2% of the crystal volume) using the SQUEEZE option of the PLATON software package.[9] Refinement of the structure converged at the following final values: R1 = 0.0866 and wR2 = 0.2182 for 1261 reflections for which $I > 2\sigma(I)$, and R1 = 0.0975 and wR2 = 0.2762 for all 1476 reflections. The largest difference peak and hole were 1.914 and −0.750 e/Å^3, respectively.

$[Ni_2(HBTC)_2(bipy)_{0.6}(dabco)_{1.4}]$, 3. Two nickel ions, two-thirds of a BTC^{3-} ligand, and four-thirds of a $H_{1.5}BTC^{1.5-}$ ligand on six different crystallographic 3-fold symmetry sites, a pillaring dabco ligand, and a pillaring bipy site were observed as an asymmetric unit of hexagonal space group *P*3. The pillaring bipy site in the asymmetric unit was statistically disordered together with two other ligated dabco sites and two lattice water sites with a total site occupancy of 1. Nickel, oxygen, and nitrogen atoms were refined anisotropically, and carbon atoms were refined isotropically. The hydrogen atoms were assigned isotropic displacement coefficients $U(H) = 1.2U(C)$, and their coordinates were allowed to ride on their respective atoms. The least-squares refinement of the structural model was performed under geometry restraints and displacement parameter restraints, such as DFIX, DANG, EXYZ, EADP, and ISOR for the dabco and bipy molecules. The final refinement was performed with modification of the structural factors for the electron densities of the disordered solvent region (2093 Å^3, 48.5% of the crystal volume) using the SQUEEZE option of the PLATON software package. Refinement of the structure converged at the following final values: R1 = 0.1172 and wR2 = 0.2531 for 3155 reflections for which $I > 2\sigma(I)$, and R1 = 0.2403 and wR2 = 0.3168 for all 10006 reflections. The largest difference peak and hole were 1.368 and −0.450 e/Å^3, respectively. The Flack parameter value of 0.47(4) that was obtained indicated that the structure is racemic twinned.

$[Ni_2(HBTC)_2(bipy)(dabco)]$, 4. Two nickel ions, two-thirds of a BTC^{3-} ligand, and four-thirds of a $H_{1.5}BTC^{1.5-}$ ligand on six different crystallographic 3 sites, a pillaring dabco ligand, and a pillaring bipy ligand were observed as an asymmetric unit of hexagonal space group *P*3. The pillaring bipy ligand is statistically disordered. All non-hydrogen atoms were refined anisotropically. The hydrogen atoms were assigned isotropic displacement coefficients $U(H) = 1.2U(C)$, and their coordinates were allowed to ride on their respective atoms. A hydrogen atom attached to a carboxylate group of a HBTC ligand was not included in the least-squares refinement of the structural model, which was performed under geometry restraints and displacement parameter restraints, such as DFIX, DANG, EXYZ, EADP, and ISOR for the disordered bipy sites. The final refinement was performed with modification of the structural factors for the electron densities of the disordered solvent region (2219 Å^3, 50.9% of the crystal volume) using the SQUEEZE option of the PLATON software package. Refinement of the structure converged at the following final values: R1 = 0.0945 and wR2 = 0.2337 for 5571 reflections for which $I > 2\sigma(I)$, and R1 = 0.1403 and wR2 = 0.2700 for all 10213 reflections. The largest difference peak and hole were 1.631 and −0.787 e/Å^3, respectively. The Flack parameter value of 0.49(3) that was obtained indicated that the structure is racemic twinned.

A summary of the crystal data for **2**−**4** is given in Tables S1−S3 of the Supporting Information. CCDC 894148, 893749, and 893750 contain the supplementary crystallographic data. The data can be obtained free of charge at http://www.ccdc.cam.ac.uk/conts/retrieving.html or from the Cambridge Crystallographic Data Centre, 12 Union Road, Cambridge CB2 1EZ, U.K.

Gas Sorption Measurements. All of the gas sorption isotherms were measured using a BELSORP-max (BEL Japan, Inc.) adsorption system employing a standard volumetric technique up to saturation pressure. The N_2 (purity of 99.999%) sorption isotherms were monitored at 77 K. The adsorption data in the pressure range of <0.1 P/P_0 were fit to the Brunauer−Emmett−Teller (BET) equation to determine the BET surface area. The entire set of adsorption data was used to obtain the Langmuir specific surface area. The H_2 (purity of 99.9999%) sorption isotherms were measured at 77 and 87 K, and the CO_2 (purity of 99.999%) and CH_4 (purity of 99.95%) sorption isotherms were measured at 195 and 273 K.

Computations. The Vienna Ab initio Simulation Package was used to calculate the ground state of many-electron systems in the framework of density functional theory.[10] The plane-wave basis set with an energy cutoff of 400 eV and the Perdew−Burke−Ernzerhof-type gradient-corrected exchange-correlation potential were employed.[11]

RESULTS AND DISCUSSION

Attempt To Synthesize the Isoreticular MOFs via the Conventional Approach. Attempts to prepare **2** and **3** via a one-pot solvothermal reaction were not successful. While the solvothermal reaction of H_3BTC with ~1.2 equiv of Ni^{II} ion in DMF at 130 °C for 3 days in the presence of an equivalent amount of bipy as a pillaring linker led to the 3D MOF, **1**, with a 3,5-connected **hms** net topology,[12] a similar solvothermal reaction in the presence of dabco as a potential pillaring linker produced only the reported 2D MOF, $[Ni(HBTC)(DMF)_2]$ (Figure S1 of the Supporting Information),[4] where the 2D sheet of the MOF made of Ni^{II} ion and HBTC ligand is the same as that of **1**, but the 3-connected nickel centers of an **hcb** net topology are ligated with two additional monodentate DMF molecules. A similar reaction but in the presence of excess amounts of dabco at ambient temperature resulted in the immediate precipitation of a cyan crystalline powder of an unidentified phase. Further solvothermal reaction of the reaction mixture with the crystalline powder in DMF solvent at 130 °C for 3 days did not indicate any phase change of the crystalline powder. An attempt to synthesize **3** via a one-pot solvothermal reaction was also unsuccessful. The product, obtained using reaction conditions similar to those for the preparation of **1** but in the simultaneous presence of the two pillaring linkers, bipy and dabco, turned out to be a heterogeneous mixture of **1** and $[Ni(HBTC)(DMF)_2]$ (Figure S2 of the Supporting Information). While bipy was incorporated as a pillaring linker in the structure of **1**, dabco was not.

PSLE of the MOF. **2** could be obtained only by soaking **1** in a dabco DMF solution via the PSLE of the structural organic linker of **1**, bipy. When the cyan single crystals of **1** were soaked in a 1.0 M dabco DMF solution at 100 °C, the crystals underwent a change in color from cyan to pale yellow (Figure 1).

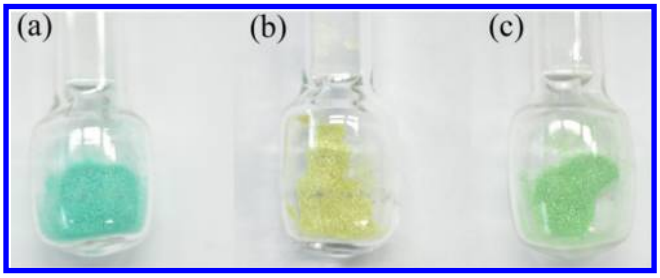

Figure 1. Optical microscopic photographs of (a) [Ni(HBTC)(bipy)] (**1**), (b) [Ni(HBTC)(dabco)] (**2**), and (c) $[Ni_2(HBTC)_2(bipy)_{0.6}(dabco)_{1.4}]$ (**3**) crystals.

To check whether the change from the cyan crystals of **1** to the pale yellow crystals of **2** is a single-crystal-to-single-crystal (SCSC) transformation, one single crystal of **1** was selected and was soaked in the same way as for the bulk crystals. The single crystal retained its crystallinity without any indication of dissolution, and there was no hint of the formation of any additional crystals. The PXRD patterns of the crystals showed gradual intensity decreases of the (*h*, *k*, *l*) reflections with a non-zero *l* index while retaining the intensities of the (*h*, *k*, 0) reflections as the soaking proceeds (Figure 2a). Two new broad peaks at $2\theta \approx 12.5°$, 25°, and 38.5°, corresponding to (0, 0, 1), (0, 0, 2), and (0, 0, 3) reflections, respectively, indicated that the *c*-axis dimension of the crystal decreased from ~11 to ~7 Å

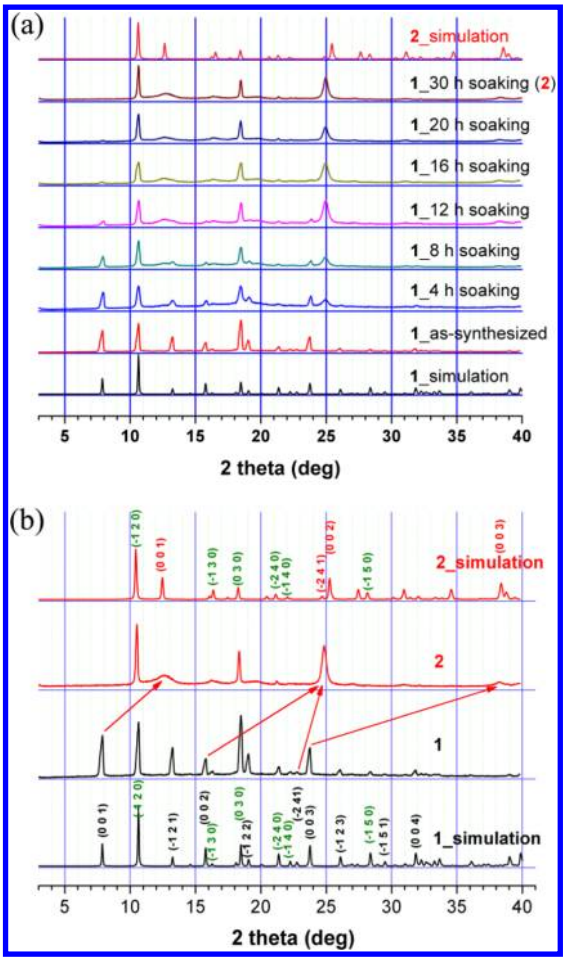

Figure 2. (a) Time-dependent PXRD patterns of approximately 10 mg of single crystals of **1** soaked in 10 mL of a 1.0 M dabco DMF solution at 100 °C. (b) PXRD patterns of the as-synthesized **1** and as-synthesized [Ni(HBTC)(dabco)] (**2**) obtained via PSM of **1** for 30 h and simulated PXRD patterns from the corresponding single-crystal structures with (*h*, *k*, *l*) indices.

while the dimensions of the *a*–*b* plane remained intact (Figure 2b). The longer bipy pillaring linkers between the 2D sheets were replaced by the shorter dabco linkers, and the replacement was completed within 30 h.

The complete exchange of pillaring ligand was confirmed by the X-ray diffraction analysis of a single crystal of **2** (Figure 3). The ~7 Å intersheet distance caused by the dabco pillaring linker agrees well with the PXRD pattern of **2**.

3 could also only be obtained by the PSLE of **1** in a DMF solution containing dabco as an additional potential pillaring ligand via partial and selective exchange of the existing pillaring ligand, bipy. Soaking the crystals of **1** in a 0.05 M dabco DMF solution at 100 °C showed a change in the color of the crystals from cyan to pale green (Figure 1). The SCSC transformation from **1** to **3** was also checked by soaking one single crystal of **1** in a 0.05 M dabco DMF solution. The PXRD patterns of the crystals of **1** soaked in the dabco solution also showed gradual intensity decreases of the (*h*, *k*, *l*) reflections with a non-zero *l* index while the intensities of the (*h*, *k*, 0) reflections were retained as the soaking proceeded, and the change to the postsynthetically modified crystals **3** was completed within 48 h (Figure 4a). New broad peaks appeared at $2\theta \approx 4.9°$, 9.8°, 14.7°, and 24.5° that could be assigned as the peaks of (0, 0, 1),

dx.doi.org/10.1021/cm303624p | *Chem. Mater.* 2013, 25, 1047–1054

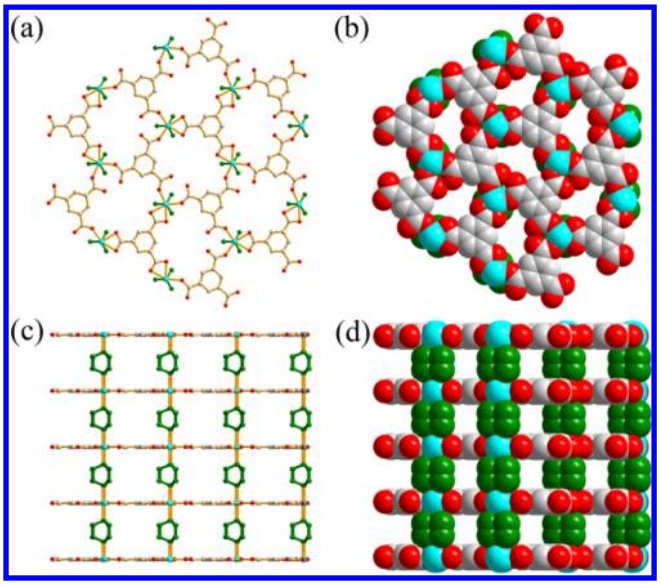

Figure 3. Crystal structure of **2**: (a) top view of the structure as a ball-and-stick diagram, (b) space-filling model showing the 2D **hcb** network structure, (c) side view of the structure as a ball-and-stick diagram, and (d) space-filling model showing the 2D sheets pillared via the dabco organic linker. Color codes: nickel, cyan; carbon, gray; oxygen, red; dabco, green.

(0, 0, 2), (0, 0, 3), and (0, 0, 5) reflections, respectively; the *c*-axis dimension of the crystal increased from ∼11 to ∼18 Å (Figure 4b). The elongated *c*-axis dimension of the crystal suggests that the alternating pillaring bipy layers have been selectively exchanged for the dabco linkers.

Although the random substitution of the pillaring ligand from bipy to dabco linker is an entropically more favorable process, the exchange in a lower-concentration dabco DMF solution occurs via the entropically less favorable selective substitution of the alternating pillaring layers. While the exchange of the pillaring ligand in a 1.0 M dabco DMF solution occurs via the random substitution of the pillaring ligand, the exchange in a 0.05 M dabco DMF solution occurs via the selective and systematic substitution of the alternating bipy/dabco pillaring layers. The single-crystal X-ray diffraction analysis showed that **3** has a $[Ni_2(HBTC)_2(bipy)_{0.6}(dabco)_{1.4}]$ structure, where the ligand exchange from bipy to dabco had occurred only in the alternating layers (Figure 5). Even though the intersheet distance pillared by bipy linkers is ∼11 Å, the occupancy factor for the bipy site in the single-crystal structure indicated that more than 60% of the bipy sites were replaced by either dabco or solvent DMF/water molecules, which agrees with the EA result.

When single crystals of **3** were soaked in a 0.1 M bipy DMF solution at ambient temperature for 7 days, there was no apparent change in the PXRD pattern of the sample. The X-ray diffraction analysis of a single crystal of the soaked sample, **4**, also showed no apparent changes in its lattice parameters or the space group. However, the structural refinement of **4** of with a formula unit of $[Ni_2(HBTC)_2(bipy)(dabco)]$ could be performed with the fully occupied bipy site in the alternating pillaring layer. The EA result also supports the formula unit of **4**.

When the crystals of **1** were soaked in a 0.3 M dabco DMF solution for 8 h at 100 °C, the PXRD pattern of the crystals showed the simultaneous appearance of the peaks related to the

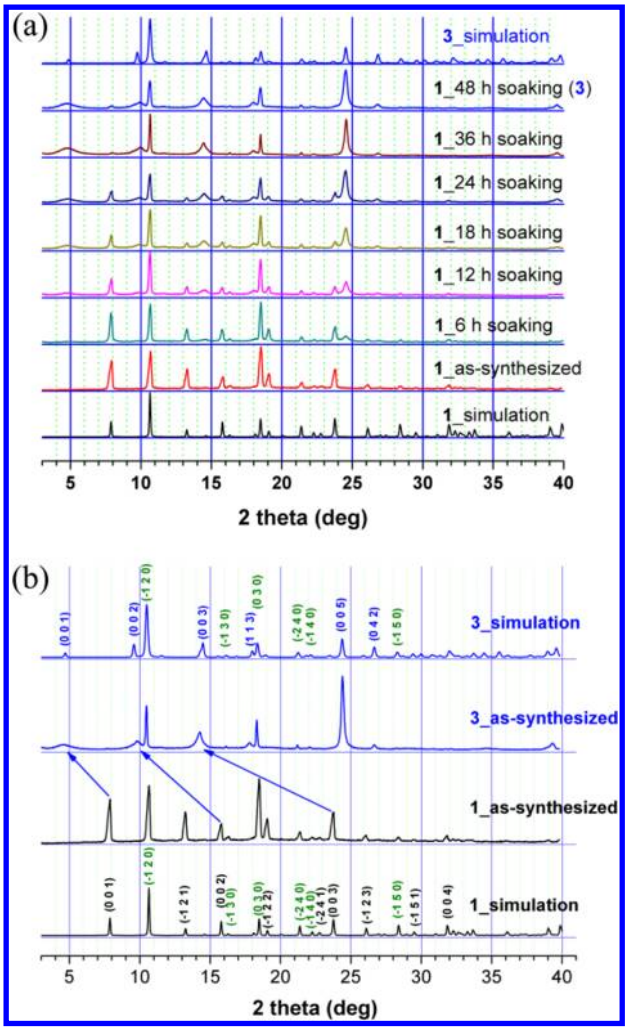

Figure 4. (a) Time-dependent PXRD patterns of approximately 10 mg of single crystals of **1** soaked in 10 mL of a 0.05 M dabco DMF solution at 100 °C. (b) PXRD patterns of as-synthesized **1** and as-synthesized $[Ni_2(HBTC)_2(bipy)_{0.6}(dabco)_{1.4}]$ (**3**) obtained via PSM of **1** for 48 h and simulated PXRD patterns from the corresponding single-crystal structures with (*h*, *k*, *l*) indices.

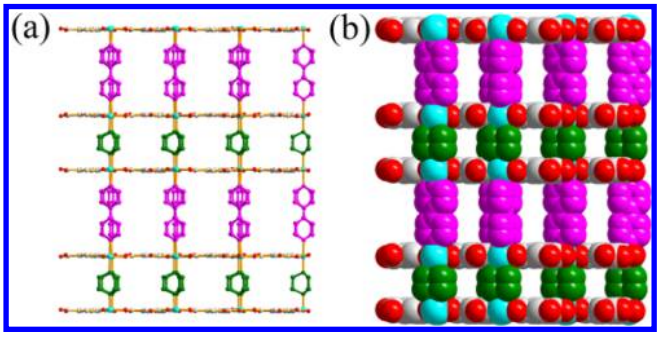

Figure 5. Crystal structure of **3**: (a) side view of the structure as a ball-and-stick diagram and (b) space-filling model showing the 2D sheets pillared via alternating bipy and dabco linkers. Color codes: nickel, cyan; carbon, gray; oxygen, red; bipy, pink; dabco, green.

structures of **1**−**3** [the peaks at $2\theta \approx 7.9°$, 15.8°, and 23.8° for (0, 0, 1), (0, 0, 2), and (0, 0, 3) reflections of **1**, respectively; the peaks at $2\theta \approx 12.6°$ and 24.6° for (0, 0, 1) and (0, 0, 2) reflections of **2**, respectively; the peaks at $2\theta \approx 4.9°$, 9.8°, 14.7°, and 25.2° for (0, 0, 1), (0, 0, 2), (0, 0, 3), and (0, 0, 5)

dx.doi.org/10.1021/cm303624p | *Chem. Mater.* 2013, 25, 1047−1054

reflections of **3**, respectively] (Figure 6). In the substitution of the pillaring linker of **1** soaked in the intermediate

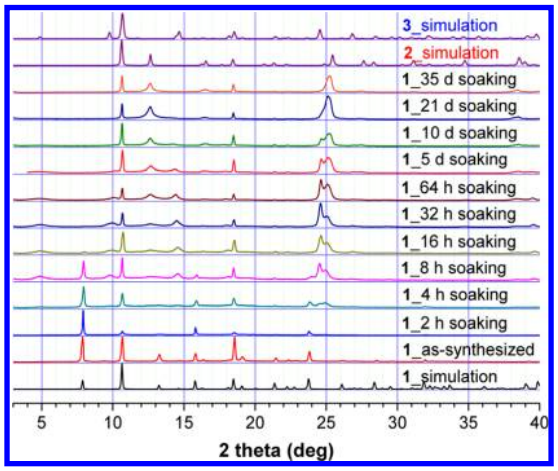

Figure 6. Time-dependent PXRD patterns of approximately 10 mg of single crystals of **1** soaked in 10 mL of a 0.3 M dabco DMF solution at 100 °C.

concentration of a dabco DMF solution, the reaction proceeds via both random substitution and systematically alternating substitution of the bipy pillaring linkers. The extended soaking of **1** in the 0.3 M dabco DMF solution for more than a month completely exchanged all bipy pillaring linkers in **1** with dabco pillaring linkers to form **2**, as in the soaking of **1** in the 1.0 M dabco DMF solution.

Reverse PSLE of the MOFs. **2** and **3** could be reversibly transformed back to **1** by simply soaking the crystals in a bipy DMF solution (Figure S3 of the Supporting Information). While the soaking of the crystals of **3** in a 0.05 M bipy DMF solution at 100 °C led to complete replacement of the pillaring dabco linker back with the bipy linker within 6 h (Figure S3b of the Supporting Information), a similar soaking of the crystals of **2** in a 0.1 M bipy DMF solution at 100 °C led to incomplete replacement of the pillaring dabco linker and generated a crystalline mixture of **1**−**3** (Figure S3a of the Supporting Information). The PXRD pattern of the mixture showed the simultaneous presence of three sets of (0, 0, *l*) reflections related to the crystals of **1**−**3**. The soaking of the crystals of **2** in a higher-concentration bipy DMF solution (1.0 M) for 1 day at 100 °C finally led to complete exchange of the pillaring linker.

Entropically and Enthalpically Favorable Pillaring Ligand Exchanges. To understand the formation of the entropically unfavorable, selectively exchanged structure **3** rather than the entropically favorable, randomly exchanged structural model **3*** (Scheme 1), we constructed three different types of 2D sheet structural models of an **hcb** net topology consisting of [bipy−Ni^{II}−bipy], [bipy−Ni^{II}−dabco], and [dabco−Ni^{II}−dabco] coordination sites (Figure 7).

While the selectively exchanged structure, **3**, contains only the [bipy−Ni^{II}−dabco] coordination site, the [bipy−Ni^{II}−bipy], [bipy−Ni^{II}−dabco], and [dabco−Ni^{II}−dabco] coordination sites can be observed in the randomly exchanged structural model, **3***. Using the total energies of the three aforementioned structural models and isolated bipy and dabco,[11] we evaluated the formation enthalpy of the coordination sites. Compared with the [bipy−Ni^{II}−bipy] coordination site, the [bipy−Ni^{II}−dabco] and [dabco−Ni^{II}−dabco] coordination sites are unfavorable by ∼11.12 and ∼34.30 kJ/mol, respectively (Figure

Scheme 1. Reaction toward 2 via Random Ligand Exchange and toward 3 via Selective Ligand Exchange

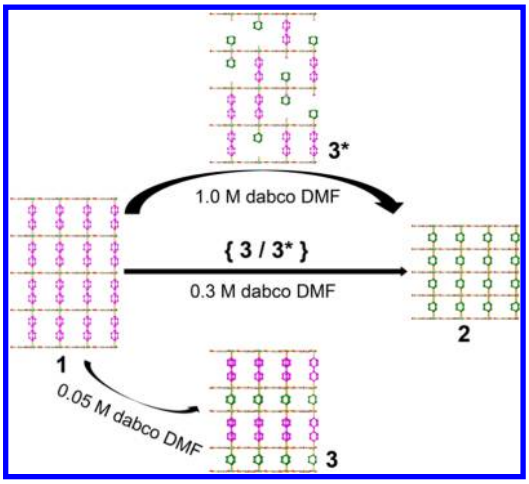

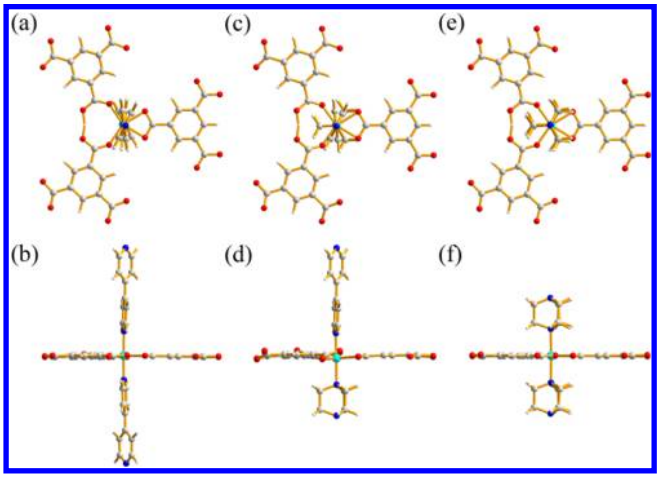

Figure 7. (a−f) Top and side views of the three different coordination sites, [bipy−Ni^{II}−bipy], [bipy−Ni^{II}−dabco], and [dabco−Ni^{II}−dabco], of the structural models consisting of 2D hexagonal lattices based on [bipy−Ni^{II}−bipy], [bipy−Ni^{II}−dabco], and [dabco−Ni^{II}−dabco] coordination sites. The Ni^{II} coordination sites in the structures with two different types of carboxylate binding modes, a chelating bindentate and two monodentate binding modes, are of a distorted octahedral geometry.

S4 of the Supporting Information). The energy difference obviously originates from the difference in the coordination strength of Ni^{II}−bipy and Ni^{II}−dabco sites. Even though dabco is a stronger base than bipy, the calculation shows that the Ni−N_{dabco} bond at the [bipy−Ni^{II}−dabco] coordination site is ∼0.15 Å more longer than the Ni−N_{bipy} bond at the [bipy−Ni^{II}−bipy] coordination site (Table 1). More interestingly, there is ∼0.05 Å more elongation of the Ni−N_{dabco} bond at the [dabco−Ni^{II}−dabco] coordination site than at the [bipy−Ni^{II}−dabco] coordination site. Similar elongations of the Ni−N_{dabco} bond were also observed in the single-crystal structures of **2**−**4**. The elongation is caused by the repulsion of the sterically more demanding ligated dabco linker with the BTC ligands. While the BTC plane in the [bipy−Ni^{II}−bipy] coordination site is almost planar, that in the [bipy−Ni^{II}−dabco] coordination site is distorted to release the strain incurred by the steric repulsion. The puckering of the BTC plane in the [dabco−Ni^{II}−dabco] coordination site is unavailable because of the symmetry, and thus, the strain originated from the steric repulsion is instead

dx.doi.org/10.1021/cm303624p | *Chem. Mater.* 2013, 25, 1047−1054

Table 1. Bond Distances (angstroms) around the Ni(II) Coordination Sites

			optimized structural model[b]		
Ni^{II} site[c]	**1**,[a] $Ni(bipy)_2$	**3**/**4** Ni(bipy)(dabco)	$Ni(bipy)_2$	Ni(bipy)(dabco)	$Ni(dabco)_2$
$Ni-N_{bipy}$	2.091	2.052/2.094	2.067	2.085	–
$Ni-N_{dabco}$	–	2.165/2.135	–	2.220	2.270
$Ni-O_b$	2.113	2.110/2.133	2.130	2.135	2.131
$Ni-O_b$	–	2.114/2.144	–	2.136	–
$Ni-O_m$	2.044	2.013/2.026	2.084	2.056	2.031
$Ni-O_m$	–	2.018/2.030	–	2.058	–
average	2.083	2.079/2.094	2.094	2.115	2.144

[a]The bond distances around the Ni(II) ion are from the reported single-crystal structure of **1**.[4] [b]Optimized 2D sheet structural models of an **hcb** net topology consisting of [bipy–Ni^{II}–bipy], [bipy–Ni^{II}–dabco], and [dabco–Ni^{II}–dabco] coordination sites. [c]$Ni(bipy)_2$ = the [bipy–Ni^{II}–bipy] coordination site. Ni(bipy)(dabco) = the [bipy–Ni^{II}–dabco] coordination site. $Ni(dabco)_2$ = the [dabco–Ni^{II}–dabco] coordination site.

released by increasing the Ni^{II}–dabco bond length. Although the random replacement of the pillaring bipy linker by dabco is entropically favorable, the formation of a [dabco–Ni^{II}–dabco] coordination site is enthalpically less favorable than the formation of a [bipy–Ni^{II}–dabco] coordination site. Hence, the selective replacement occurs as an enthalpically favorable process in the lower-concentration dabco DMF solution.

Attempts To Interconvert the Entropically and Enthalpically Favorable Pillaring Ligand Exchange Processes. To find out whether the entropically favorable random exchange in the higher-dabco concentration solution could be converted to an enthalpically favorable selective exchange, the reaction temperature was lowered to 40 °C with no indication of the formation of the enthalpically favorable product, **3**. At temperatures lower than 40 °C, no appreciable exchange reaction occurred over a period of more than 1 week. Similarly, to find out whether the enthalpically favorable selective exchange could be converted to an entropically favorable random exchange, the reaction temperature was increased to 200 °C in an autoclave. There was no indication of the formation of the entropically favorable product. The entropic contribution of the reaction is probably not large enough to convert the reaction process in the experimentally allowed temperature range.

N_2 Sorption Behaviors of the MOFs. The gas sorption behavior of the isoreticular MOFs, activated **1a**–**3a**, were investigated. The pore dimensions and the specific surfaces areas were accessed using N_2 sorption isotherms (Figure 8).

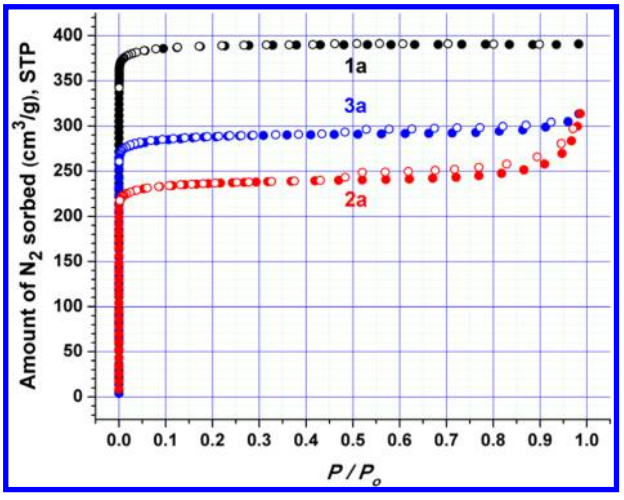

Figure 8. N_2 sorption isotherms of **1a**, **2a**, and **3a** at 77 K.

The N_2 uptake amount and the BET specific area of **2a** are 251 cm^3/g and 930 m^2/g, respectively, which are significantly smaller than those of **1a** (391 cm^3/g and 1540 m^2/g,[13] respectively). The complete exchange of the longer pillaring ligand bipy by the shorter pillaring ligand dabco in **2a** significantly reduced the pore volume and the specific surface area. The partial exchange of the pillaring ligand by the shorter pillaring ligand dabco in **3a** also led to a reduced N_2 uptake amount and BET surface area compared with those of **1a**. The N_2 uptake amount and the BET specific area of **3a** were 305 cm^3/g and 1150 m^2/g, respectively. As expected from the intermediate dimension with the selectively and alternatively exchanged mixed pillars, these values are smaller than those of **1a** with pure bipy pillar, but larger than those of **2a** with pure dabco pillar. All the activated samples, **1a**–**3a**, are stable in air at least for a couple of hours. The activated samples exposed in air for a couple of hours did not indicate any decrease in N_2 uptake amounts. However, an extended exposure in air or a soaking in water led to the complete loss of the crystallinity and the porosity of the activated samples. The activated samples exposed to air for one month or soaked in water overnight did not show any powder diffraction peaks and did not adsorb any N_2 at 77 K.

CO_2 and CH_4 Sorption Behaviors of the MOFs. The effects of the modified pore dimensions of **2a** and **3a** compared with that of **1a** are reflected in the sorption behavior of CH_4 and CO_2 (Figures 9 and 10 and Figures S4 and S5 of the Supporting Information). At 195 K, decreased CH_4 uptake amounts on **2a** and **3a** (106 and 118 mg/g, respectively) were observed compared with that of **1a** (152 mg/g) (Figure 9 and Figure S5 of the Supporting Information). However, at 273 K, slightly increased uptake amounts on **2a** and **3a** were observed compared with that on **1a** (Figure 9a). The larger CH_4 sorption

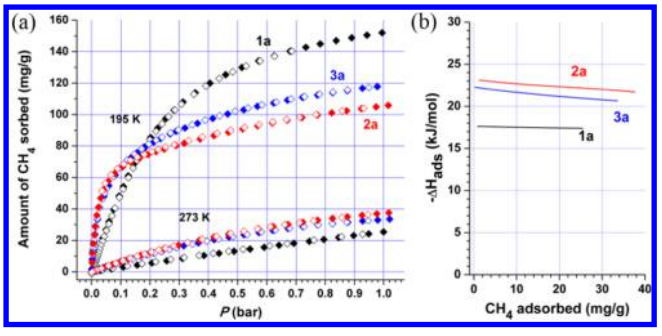

Figure 9. (a) CH_4 sorption isotherms of **1a** (black), **2a** (red), and **3a** (blue) at 195 and 273 K and (b) their adsorption enthalpies.

dx.doi.org/10.1021/cm303624p | Chem. Mater. 2013, 25, 1047–1054

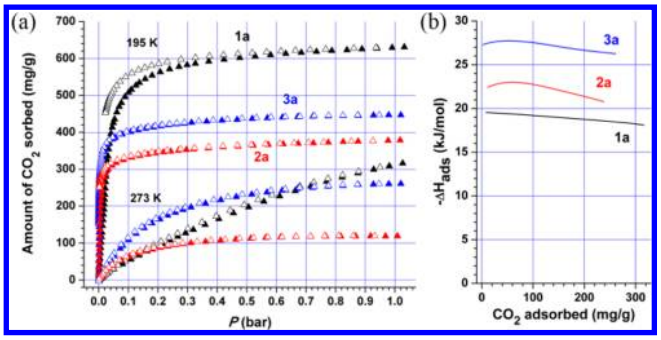

Figure 10. (a) CO_2 sorption isotherms of **1a** (black), **2a** (red), and **3a** (blue) at 195 and 273 K and (b) their adsorption enthalpies.

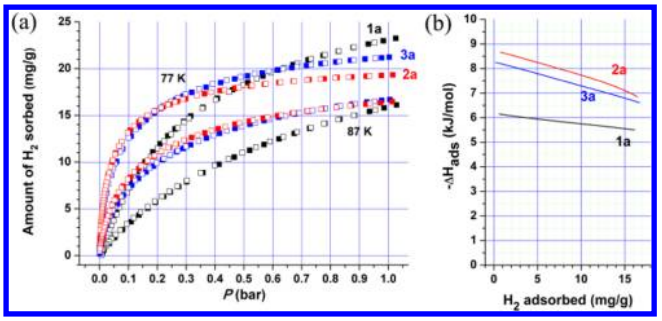

Figure 11. (a) H_2 sorption isotherms of **1a** (black), **2a** (red), and **3a** (blue) at 77 and 87 K and (b) their adsorption enthalpies.

uptake amounts at 273 K on **2a** and **3a** with the smaller pore volumes compared with that on **1a** with the larger pore volume are due to the larger CH_4 adsorption enthalpy on **2a** and **3a** (approximately −21 and −23 kJ/mol, respectively) than that on **1a** (approximately −17 kJ/mol) (Figure 9b). On the other hand, at 273 K, the CH_4 uptake amount on **2a** (38 mg/g) is similar to that on **3a** (34 mg/g) even though the pore volume of **2a** is significantly larger than that of **3a**.

The sorption behavior of CO_2 on **1a**−**3a** is different from that of CH_4 (Figure 10 and Figure S6 of the Supporting Information). The qualitative uptake behavior of CO_2 on **1a**−**3a** looks similar to that of CH_4 (Figure 10a). Although, at 195 K, the CO_2 uptake amount on **3a** (447 mg/g) is ∼1.2 times that on **2a** (379 mg/g), at 273 K the CO_2 uptake amount on **3a** (261 mg/g) is ∼2.2 times that on **2a** (119 mg/g), which is caused by the larger CO_2 adsorption enthalpy on **3a** (approximately −27 kJ/mol) than that on **2a** (approximately −22 kJ/mol) (Figure 10b). Although the pore dimension of **3a** based on the N_2 uptake amount is larger than that of **2a**, the adsorption enthalpy of **3a** on CO_2 is larger than that of **2a**, which is due to the combined effects of the different properties of the pillaring ligands and of the unsaturated metal sites generated from the solvent or monodentate dabco-ligated Ni(II) centers in **3a**. The less hydrophobic nature of aromatic bipy and aliphatic dabco as mixed pillaring ligands in **3a** compared to that of pure aliphatic dabco in **2a** is responsible for the larger adsorption enthalpy of CO_2 with a larger polarizability and quadrupole moment on **3a** than **2a**. In addition, the presence of the unsaturated metal sites is also contributing to the larger adsorption enthalpy of **3a** versus that of **2a**. At 1 bar and 273 K, the CO_2 uptake amount of **1a** is 316 mg/g, which is the second largest amount yet reported at this temperature,[14a] and almost comparable with the largest amount of SNU-5, 385 mg/g.[14b] More interestingly, although the uptake amount of **3a** at 1 bar and 273 K is smaller than those of **1a** and SNU-5, the uptake amount at ∼0.15 bar (which is the partial pressure of CO_2 in flue gas), 141 mg/g, is almost twice the uptake amounts of **1a** and SNU-5 at the same pressure, 72 and 73 mg/g, respectively.

H_2 Sorption Behaviors of the MOFs. At 77 K, interestingly, although the specific surface areas and the pore dimensions of **2a** and **3a** were significantly reduced compared with those of **1a**, the H_2 uptake amounts of **2a** and **3a** (19.5 and 21.1 mg/g, respectively) were only slightly reduced compared with that of **1a** (23.1 mg/g) (Figure 11a). At 87 K, more interestingly, the H_2 uptake amounts of **2a** and **3a** (16.5 and 16.6 mg/g, respectively) are even slightly larger than that of **1a** (16.0 mg/g). The increased adsorption enthalpies of **2a** and **3a** (Figure 11b), which come from the more extensive interaction of the adsorbate H_2 with the pore surface of the reduced pore dimensions, are responsible for the H_2 sorption behaviors.[15] Surprisingly, the H_2 adsorption enthalpy of **2a** with no unsaturated metal sites is slightly larger than that of **3a** with the unsaturated metal sites. The interaction of H_2 with the pore surface of **2a** with the smaller pore dimension compared with that of **3a** with the larger pore dimension is responsible for the slightly larger H_2 adsorption enthalpy of **2a** versus that of **3a**.

■ CONCLUSIONS

The preparations of the two isoreticular MOFs, **2** and **3**, which cannot be attained via the conventional synthetic approach, were demonstrated via the PSLE of **1**. By soaking **1** in a high-concentration dabco DMF solution, we completely exchanged all of the aromatic bipy pillaring linkers in **1** with the shorter aliphatic dabco pillaring linkers to form the isoreticular 3D MOF, **2**, with reduced pore dimensions and a reduced volume. The reaction proceeded via the entropically favorable random substitution of the pillaring linker. This reaction process is enthalpically unfavorable because of the formation of the sterically more demanding [dabco−Ni^{II}−dabco] coordination site. In contrast, the soaking of **1** in a low-concentration dabco DMF solution led to the enthalpically favorable isoreticular MOF, **3**, with the partially and selectively exchanged additional component, dabco linker. Even though the reaction toward selectively exchanged **3** is entropically less favorable than that toward randomly exchanged **3***, **3** with no [dabco−Ni^{II}−dabco] coordination site is responsible for the enthalpically favorable exchange process.

The series of MOFs (**1** with all aromatic bipy linkers, **2** with all aliphatic dabco linkers, and **3** with both aromatic and aliphatic pillaring linkers) provided an opportunity to assess the relationship between the pore dimension and hydrophobicity of the pore surface and the adsorption enthalpies of adsorbates. The CH_4 adsorption enthalpy increases as the pore dimension decreases because of the more extensive interaction of the adsorbate with the pore surface with reduced pore dimensions. As expected, **2**, with the smallest pore dimensions, showed the largest CH_4 adsorption enthalpy, and **1**, with the largest pore dimensions, showed the smallest CH_4 adsorption enthalpy. However, **3**, with an intermediate pore dimension and mixed pore surface properties, showed the largest CO_2 adsorption enthalpy. The adsorption enthalpy is affected not only by the pore dimension but also by the pore surface properties.

Postsynthetic exchanges of a ligand involved in the network connectivity can be used as a general strategy for the preparation of isoreticular MOFs that are difficult to obtain

dx.doi.org/10.1021/cm303624p | Chem. Mater. 2013, 25, 1047−1054

or even cannot be attained via the conventional solvothermal reaction.

■ ASSOCIATED CONTENT

Supporting Information

CIF files for **2**–**4**; tables of the crystal data and structure refinement for **2**–**4**; PXRD patterns of the products obtained via conventional one-pot reactions of H_3BTC, Ni^{II}, and dabco and H_3BTC, Ni^{II}, bipy, and dabco; PXRD patterns of the products obtained via reverse PSLE of **2** and **3**; and CH_4 and CO_2 sorption isotherms of **1a**–**3a** at 195 and 273 K, respectively. This material is available free of charge via the Internet at http://pubs.acs.org.

■ AUTHOR INFORMATION

Corresponding Author

*E-mail: mslah@unist.ac.kr.

Notes

The authors declare no competing financial interest.

■ ACKNOWLEDGMENTS

This work was supported by NRF-2010-0019408, NRF-2012R1A2A2A01003077, and WCU programs (R31-20012) through the National Research Foundation of Korea.

■ ABBREVIATIONS

BET, Brunauer–Emmett–Teller; bipy, 4,4′-bipyridine; 2D, two-dimensional; 3D, three-dimensional; dabco, 1,4-diazabicyclo[2.2.2]octane; DMF, *N*,*N*′-dimethylformamide; EA, elemental analysis; H_3BTC, 1,3,5-benzenetricarboxylic acid; MOFs, metal–organic frameworks; PSLE, postsynthetic ligand exchange; PSM, postsynthetic modification; PXRD, powder X-ray diffraction; SCSC, single-crystal-to-single-crystal

■ REFERENCES

(1) Cohen, S. M. *Chem. Rev.* **2012**, *112*, 970–1000.
(2) (a) Das, S.; Kim, H.; Kim, K. *J. Am. Chem. Soc.* **2009**, *131*, 3814–3815. (b) Song, X.; Kim, T. K.; Kim, H.; Kim, D.; Jeong, S.; Moon, H. R.; Lah, M. S. *Chem. Mater.* **2012**, *24*, 3065–3073. (c) Huang, S.; Li, X.; Shi, X.; Hou, H.; Fan, Y. *J. Mater. Chem.* **2010**, *20*, 5695–5699. (d) Prasad, T. K.; Hong, D. H.; Suh, M. P. *Chem.—Eur. J.* **2010**, *16*, 14043–14050. (e) Dincâ, M.; Long, J. R. *J. Am. Chem. Soc.* **2007**, *129*, 11172–11176. (f) Mi, L.; Hou, H.; Song, Z.; Han, H.; Xu, H.; Fan, Y.; Ng, S. W. *Cryst. Growth Des.* **2007**, *7*, 2553–2561. (g) Mi, L.; Hou, H.; Song, Z.; Han, H.; Fan, Y. *Chem.—Eur. J.* **2008**, *14*, 1814–1821.
(3) (a) Burnett, B. J.; Barron, P. M.; Hu, C.; Choe, W. *J. Am. Chem. Soc.* **2011**, *133*, 9984–9987. (b) Kim, M.; Cahill, J. F.; Su, Y.; Prather, K. A.; Cohen, S. M. *Chem. Sci.* **2012**, *3*, 126–130.
(4) Gao, C.; Liu, S.; Xie, L.; Ren, Y.; Cao, J.; Sun, C. *CrystEngComm* **2007**, *9*, 545–547 . Here and in the reference, **1** is formulated as [Ni(HBTC)(bipy)]; however, the correct formulation for **1** is $[Ni_3(BTC)(H_{1.5}BTC)_2(bipy)_3]$, because the H_3BTC ligands in the framework of **1** are in three different deprotonated states. One is in the form of a fully deprotonated BTC^{3-} state, and the others are in the form of partially deprotonated H_2BTC^{-}/$HBTC^{2-}$ states. The ligands in the partially deprotonated H_2BTC^{-}/$HBTC^{2-}$ states are involved in interligand hydrogen bonding in the 2D sheet with an **hcb** net topology.
(5) *Materials Studio*, version 4.3; Accelrys: San Diego, 2008.
(6) *Rapid Auto*, R-Axis series, catalog no. 9220B101, Rigaku Corp.
(7) Burla, M. C.; Caliandro, R.; Camalli, M.; Carrozzini, B.; Cascarano, G. L.; De Caro, L.; Giacovazzo, C.; Polidori, G.; Siliqi, D.; Spagna, R. *J. Appl. Crystallogr.* **2007**, *40*, 609–613.
(8) Sheldrick, G. M. *SHELXTL-PLUS, Crystal Structure Analysis Package*; Bruker Analytical X-ray: Madison, WI, 1997.
(9) Spek, A. L. *Acta Crystallogr.* **1990**, *A46*, 194–201.
(10) (a) Hohenberg, B.; Kohn, W. *Phys. Rev.* **1964**, *136*, B864–B871. (b) Kohn, W.; Sham, L. J. *Phys. Rev.* **1965**, *140*, A1133–A1138. (c) Kresse, G.; Furthmüller, J. *Phys. Rev. B* **1996**, *54*, 11169–11186. (d) Kresse, G.; Furthmüller, J. *Comput. Mater. Sci.* **1996**, *6*, 15–50.
(11) Perdew, J. P.; Burke, K.; Ernzerhof, M. *Phys. Rev. Lett.* **1996**, *77*, 3865–3868.
(12) Blatov, V. A. *IUCr CompComm Newsletter* **2006**, *7*, 4. TOPOS is available at http://www.topos.ssu.samara.ru/.
(13) Even though the sample of **1** was activated according to the reported procedure at 150 °C under vacuum for 12 h, the N_2 uptake amount and the BET specific area of **1a** are significantly larger than the reported values, 290 cm^3/g and 970 m^2/g, respectively.[4] However, the pore volume calculated from the N_2 uptake amount of **1a**, 0.605 cm^3/g, is still slightly smaller than that calculated from the solvent cavity volume of the reported single-crystal structure of **1**, 0.700 cm^3/g.
(14) (a) Sumida, K.; Rogow, D. L.; Mason, J. A.; McDonald, T. M.; Bloch, E. D.; Herm, Z. R.; Bae, T.-H.; Long, J. R. *Chem. Rev.* **2012**, *112*, 724–781. (b) Lee, Y.-G.; Moon, H. R.; Cheon, Y. E.; Suh, M. P. *Angew. Chem., Int. Ed.* **2006**, *45*, 916–920.
(15) (a) Suh, M. P.; Park, H. J.; Prasad, T. K.; Lim, D.-W. *Chem. Rev.* **2012**, *112*, 782–835. (b) Zhao, D.; Yuan, D.; Zhou, H.-C. *Energy Environ. Sci.* **2008**, *1*, 222–235.